ADVANCED
OPTICAL
MATERIALS

Supporting Information

for *Adv. Optical Mater.,* DOI: 10.1002/adom.202202649

Gold Au(I)$_6$ Clusters with Ligand-Derived Atomic Steric Locking: Multifunctional Optoelectrical Properties and Quantum Coherence

Sourov Chandra, Alice Sciortino, Susobhan Das, Faisal Ahmed, Arijit Jana, Jayoti Roy, Diao Li, Ville Liljeström, Hua Jiang, Leena-Sisko Johansson, Xi Chen,* Nonappa, Marco Cannas, Thalappil Pradeep, Bo Peng, Robin H. A. Ras, Zhipei Sun, Olli Ikkala,* and Fabrizio Messina**

Supporting Information

Gold Au(I)$_6$ clusters with ligand-derived atomic steric locking: Multifunctional optoelectrical properties and quantum coherence

Sourov Chandra[1]*, Alice Sciortino[2,3], Susobhan Das[4], Faisal Ahmed[4], Arijit Jana[5], Jayoti Roy[5], Diao Li[4], Ville Liljeström[6], Hua Jiang[1,6], Leena-Sisko Johansson[7], Xi Chen[1]*, Nonappa[8], Marco Cannas[2], Thalappil Pradeep[5], Bo Peng[1], Robin H. A. Ras[1], Zhipei Sun[4,9], Olli Ikkala[1]* and Fabrizio Messina[2,3]*

[1] Department of Applied Physics, Aalto University, P. O. Box 15100, Espoo, FI-00076 Aalto, Finland.

[2] Dipartimento di Fisica e Chimica - Emilio Segrè. Università degli Studi di Palermo. Via Archirafi 36, 90123 Palermo, Italy.

[3] CHAB - ATeN Center, Università degli studi di Palermo, viale delle scienze, Edificio 18, 90128, Palermo, Italy.

[4] Department of Electronics and Nanoengineering, Aalto University, FI-00076 Aalto, Finland.

[5] Department of Chemistry, DST Unit of Nanoscience (DST UNS) and Thematic Unit of Excellence (TUE), Indian Institute of Technology Madras, Chennai 600036, India.

[6] Nanomicroscopy Center, OtaNano, Aalto University, FI-00076 Aalto, Finland.

[7] Department of Bioproducts and Biosystems, School of Chemical Engineering, Aalto University, FI-00076 Aalto, Finland.

[8] Faculty of Engineering and Natural Sciences, Tampere University, P. O. Box 541, Tampere, FI-33101 Finland.

[9] QTF Centre of Excellence, Department of Applied Physics, Aalto University, FI-00076 Aalto, Finland.

EXPERIMENTAL SECTION

Materials

$HAuCl_4.3H_2O$, methanol, ethanol, dichloromethane (DCM), ascorbic acid, sodium borohydride ($NaBH_4$), DCM-d_2 and sodium acetate were purchased from Sigma-Aldrich and used as received. The ligand, 6-(Dibutylamino)-1,3,5-triazine-2,4-dithiol was acquired from TCI Europe N.V. Ultrapure Milli-Q water (18 Ω) was used in our experiments.

Synthesis of gold nanoclusters

The synthesis of GNCs were performed using $HAuCl_4$ and 6-(Dibutylamino)-1,3,5-triazine-2,4-dithiol (TRZ) as the precursors. Briefly, 20 mg of $HAuCl_4$ was dissolved in 5 mL of methanol in a closed glass vial (20 mL) at room temperature (~22 °C). To the mixture, 7 mL of DCM was added. A solution containing 23.5 mg of TRZ ligand in 2 mL of DCM was added to the above mixture with vigorous stirring. The pale-yellow solution of $HAuCl_4$ was immediately turned to bright red in colour. After few minutes (~10-15 minutes) of stirring the colour of the solution gradually transformed to yellow. Then the reducing agents, either ascorbic acid (45 mg in 1 mL of water) or $NaBH_4$ (2 mg in 1 mL of water) was added to the solution. The reaction mixture was stirred for 12 hours at room temperature (~22 °C). The solvent was removed under reduced pressure using a rotary evaporator at 30 °C. The residue was washed with ethanol to remove the excess ligand and the reducing agent. Finally, the product was separated by centrifugation at 5000 rpm for 30 mins and dried in air after discarding the ethanol. The clusters were stored in a refrigerator at 4 °C for further use.

X-ray photoelectron spectroscopy (XPS)

X-ray photoelectron spectroscopy was performed in Kratos Axis Ultra ESCA X-ray photoemission spectrometer using AlKα irradiation at low power (100 W) and under neutralization. The X-ray source was operated at 8 mA and 12.5 kV and the analyzer pass energy was 20 eV for high resolution scans and 80 eV for the survey spectra. The pressure in the analysis chamber was about 8×10^{-8} Pa during the measurements. The binding energy (BE) scale was referenced to 284.8 eV as determined by the location of the maximum peak on the C1s spectra, associated with adventitious carbon. The accuracy of the BE determined with respect to this standard value was within ±0.1 eV.

STEM analysis

STEM images were captured by using JEM-2200FS Double Cs-corrected transmission electron microscope. The instrument was operated at an acceleration voltage of 200 kV with field-emission guns. Specimen for STEM analyses were prepared by drop-casting from the solution of GNCs in DCM over the ultrathin-carbon (<10 nm thickness) coated copper grids. The samples were incubated for 1 min, after which the excess material was removed by washing with ethanol.

ESI Mass spectroscopy

High resolution mass spectrum was carried out using SYNAPT G2-Si High Definition MS (HDMS) system. It is equipped with an electrospray ionization source, step wave ion transfer optics and a quadrupole mass filter. Sodium acetate is used as an ionization enhancer during the measurement. The spectrum was collected in negative and positive ion mode following an optimized condition of flow rate 20 µL/ml, capillary voltage 2.5 - 3 kV, spray current 100 - 120 nA, cone voltage 0 V, source voltage 70-100 °C. The collision energy-dependent fragmentation studies were performed after selecting the molecular ion (at m/z = 2025.28) trapped inside the ion mobility cell.

^{1}H-NMR Spectroscopy

^{1}H-NMR spectra were recorded using Bruker AV III 400 spectrometer operating at 400 MHz for ^{1}H. For sample preparation, dried GNC-1 and TRZ ligand were dissolved in dichloromethane-d_2.

Measurement of refractive index

Refractive index measurements were performed using J. A. Woollam M-2000UI spectroscopic ellipsometer. Thin layer of the samples was prepared by spin coating over a silicon wafer.

Absolute quantum yield measurement

The absolute PL quantum yield was measured using a C9920-03G system equipped with a 150W xenon lamp (Hamamatsu Photonics Co. Ltd., Japan).

Small angle X-ray scattering (SAXS) measurements

X-ray diffraction measurements were performed to complement the structural characterization of the nanoclusters. The measurements were carried out from dried samples. The gold nanocluster-DCM solution was dried to form a powder, which was confined between thin Kapton films. The

X-ray diffraction measurement was carried out in perpendicular transmission geometry with the Xenocs Xeuss 3.0 system using Cu K-α radiation (multilayer monochromator, λ=1.542 Å, parallel beam collimation). The samples were measured in a vacuum and the background scattering from the Kapton films was subtracted. The final model was calculated using Powder Cell software[1]. The diffraction peaks of the NCs have been analyzed by comparing the plausible structure factors (lattices) and calculating a full diffraction pattern.

Steady-state optical measurements

Steady-state absorption measurements were carried out on GNCs dispersed in dichloromethane within a 1 cm quartz cuvette, using a double beam spectrophotometer (JASCO V-560) in the 220−700 nm range.

Steady-state emission

The emission spectra have been collected on diluted suspensions of GNCs in dichloromethane (absorption < 0.2 OD at the excitation wavelength) by a JASCO FP-6500 spectrofluorometer in a 1 cm cuvette with a 3 nm resolution bandwidth.

Nanosecond time-resolved fluorescence

The emission decay kinetics were recorded by exciting the samples by laser pulses of 0.1−0.3 mJ energy and 5 ns duration, obtained from a tunable laser (410-700 nm), and dispersing their photoluminescence on an intensified CCD camera. The camera was triggered to acquire spectra within windows of variable widths (0.5 ns – 0.5 ms) and delays from the laser pulse. Decay kinetics were obtained by spectrally integrating the photoluminescence signal and analysing it as a function of delay time. The decay curves were fitted by a bi-exponential kinetics in the form: $A \exp[-t/t_1] + B \exp[-(t/t_2)^{b}]$. In this expression, b is a stretching parameter (estimated to be 0.8 by the fit), that we find necessary to satisfactorily reproduce the experimental data, suggestive of the presence of a statistical distribution of different lifetimes around t_2.

Femtosecond transient absorption (TA)

TA measurements in a pump/probe geometry were carried out on a home-built setup, described in previous publication[2]. The setup is pumped by a 5 kHz Ti:sapphire femtosecond amplifier (Spectra Physics Solstice-Ace), which produces 50 fs pulses peaking at 800 nm (FWHM = 30 nm) with 350 mJ energy per pulse. The fundamental beam is split 80%/20% by a beam splitter to generate the pump and the probe, respectively. The pump at 400 nm was obtained by frequency-doubling the fundamental in an ultrathin β-BBO crystal (250 mm) in order to create a 400 nm beam (20% efficiency), which is isolated from the fundamental by a Schott BG40 filter. The typical pump intensity was 50-100 nJ/pulse. This beam was chopped at 500 Hz and focused on the sample by a parabolic beam with f = 150 mm, while its polarization is controlled by a waveplate.

On the second arm, white light is generated focusing the 800 nm beam in a 1 mm quartz cuvette containing D_2O, generating a broadband pulse extending from 400 to 750 nm. The probe is focused on the sample by the same parabolic mirror used to focus the pump. The pump–probe delay is controlled by a motorized delay stage. The probe and the pump overlap within the sample, which continuously flows in a 0.2 mm thick flow cell. After the sample, the probe beam is dispersed by a home-built monochromator (resolution = 3 nm) onto a camera detector system with 1024 pixels (Glaz Linescan-I) with single-shot capability. A typical signal is obtained by averaging 5000 pumped and 5000 unpumped spectra for each delay and scanning over the pump–probe delay 10–20 times. The measurements were carried out under magic angle detection conditions. The data presented in the paper were subjected to standard correction procedures, which eliminate the effects of cross-phase modulation and group velocity dispersion (GVD). The temporal resolution is about 70 fs for measurements pumped at 400 nm.

TA kinetics at different wavelengths were initially fitted by multi-exponential decay kinetics convoluted to a Gaussian instrumental response function, obtaining the fits shown in Figure 4c and Figure 4d. The fit residuals were processed by FFT in order to analyse the oscillatory behaviour of the TA signal. The time-frequency analysis of the fit residuals was obtained by calculating the short-time Fourier transform within a Hann moving window with 800 fs width (that is, about twice the period of Au-Au oscillations).

Third harmonic generation experiment and setup

The dry GNC-1 powder was dispersed in dichloromethane. The transparent films were then prepared by drop-casting the dispersion over a clean glass slide and allowed to dry under ambient conditions. The thin film over the glass slide has been analysed as the sample for non-linear optical responses. We use an ultrafast laser for the measurement. An optical parametric amplifier (Spectra-Physics, TOPAS) with a repetition rate of 2 kHz is used to generate the light pulses. The wavelength range of the light beam comes from the optical parametric amplifier, which is tuneable from 0.8μm to 1.6 μm. The pulse width of light pulses is ~230 fs. The beam is focused onto the sample with an objective (NA=0.75, 40X). The spot sizes of the Gaussian beam (FWHM) over the samples are ~2.5 μm. The reflected light is separated from the input light using filters and measured with a photo multiplier tube following a monochromator (Andor 328i). The THG signal has been measured under ambient temperature (~ 25°C) with an average incident power of ~1μW (28.84 GW/cm^2 intensity).

Device Fabrication

The device preparation started with mechanically exfoliating WSe_2 flakes using standard scotch-tape technique from a commercial bulk source (2D Semiconductors) over *p*-doped silicon substrate (0.001 – 0.005 Ω·cm) covered with a 285 nm thick SiO_2. The electron beams sensitive polymer (PMMA A4.5) was spin coated, and the electrodes were patterned *via* electron beam lithography (EBL Vistec, EPBG5000pES) over targeted flakes in desired geometry. The metallization of 5 nm Ti adhesion layer followed by 50 nm thick Au was carried out by electron beam evaporator (MASA IM-9912) at ~ 10^{-7} torr chamber pressure. The electrical measurements were performed with a custom-built setup based on a Linkam LN600-P probe station with the source-measure unit (Keithley 2400) and multiplexing/voltage measurement unit (Keithley 2700). GNC-1 dispersions in DCM with concentration 0.1, 0.37 and 0.5 mg/mL were drop-casted over WSe_2 in such a way that the device is fully covered by the solution.

Atomic force microscopy (AFM)

The topographic image and thickness of WSe_2 flakes were collected by Bruker, Dimension Icon atomic force microscope.

DFT and TDDFT simulations

In this work, the GPAW software package[3] was applied to do all the calculations. The structure optimizations were done using the GPAW grid mode with the real-spacing h=0.2 Å. The $Au(I)_6(TRZ)_3$ clusters was placed into a cubic unit cell with a vacuum size 6 Å added to the cluster's edge at each dimension. The geometry was considered to be converged when the maximum residual force was below 0.05 eV/Å. A hexagonal unit cell of WSe_2 from materalproject.org (DOI:10.17188/1192989) was repeated 4 times in z direction to build an 8-layer model for the WSe_2 simulation. Periodic conditions were applied in x and y directions, while the

8 Å vacuum was added to both sides of the surface in z direction. 8*8*1 K-points were used for the simulation.

Perdew-Burke-Ernzerhof (PBE) functional was used for the exchange-correlation energy[4], and the van der Waals interactions were described by the Tkatchenko-Scheffler model[5]. Per atom, the electronic configuration of valence electrons is H($1s^1$) C($2s^2 2p^2$), S($3s^2 3p^4$), N($2s^2 2p^5$) and Au ($5d^{10} 6s^1$). The remaining electrons were treated as a frozen core. The default PAW dataset package 0.9.20000 was used for all the atoms.

The optical absorption spectrum were computed by the real-time-propagation time-dependent density functional theory (RT-TDDFT) implemented in GPAW with PBE functionals and LCAO (Linear Combination of Atomic Orbitals) mode[6]. In the LCAO mode, the default GPAW double-zeta polarized (dzp) basis sets were used for C, H, N, S, while the optimized double-zeta basis set (so- called "p-valence" basis set) was picked for Au atoms. In the RT-TDDFT simulation, the propagation was carried out up to T=30.0 fs in steps of 5.0 as. The real-spacing h=0.3 and vacuum size 8 Å were chosen for the RT-TDDFT calculations. The work-function of the clusters are calculated based on the method elsewhere[7].

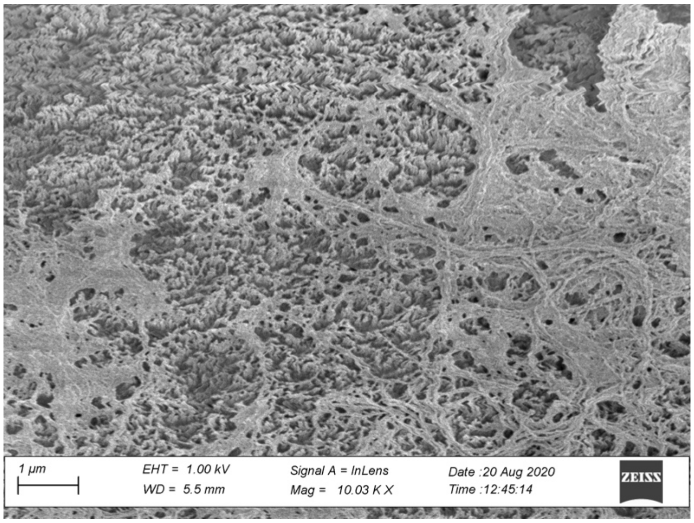

Figure S1. The reaction of 6-(dibutylamino)-1,3,5-triazine-2,4-dithiol (TRZ) with $HAuCl_4$ leads to complexation with fibrillar poorly defined assemblies, demanding another second reduction step by ascorbic acid to allow the final ultrasmall well defined nanoclusters.

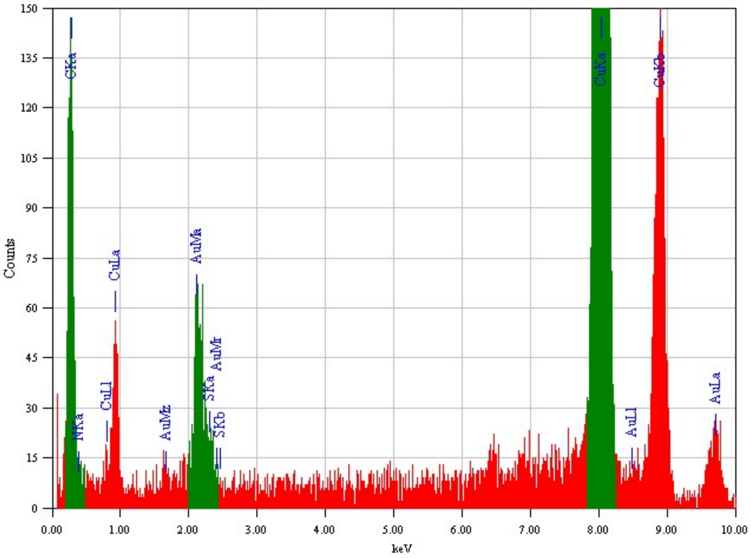

Figure S2. EDX spectrum of GNC-1.

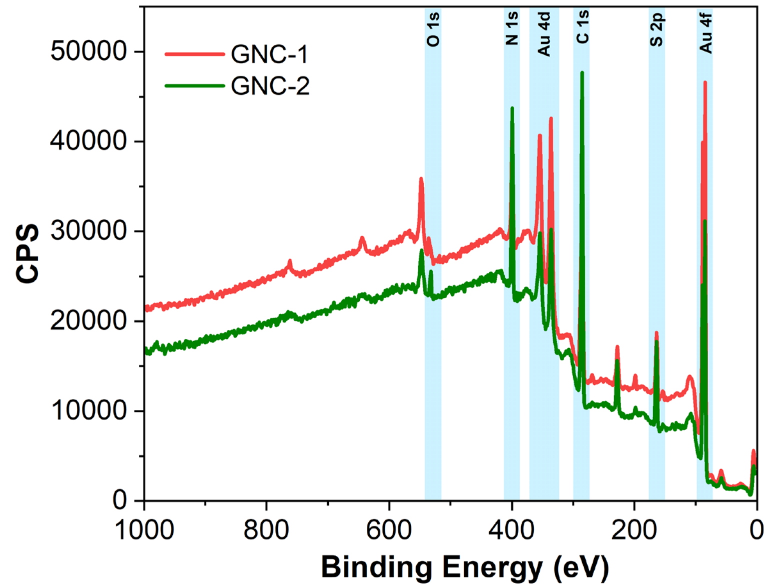

Figure S3. Full-width XPS spectra of GNC-1 and GNC-2.

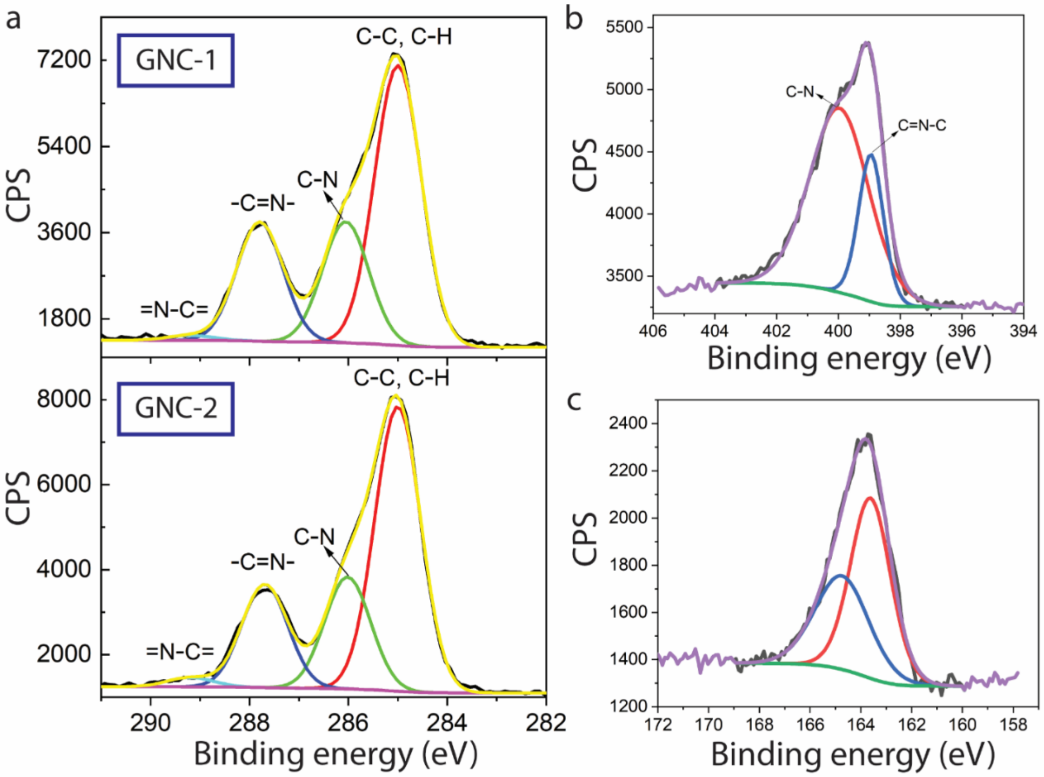

Figure S4. (a) C1s XPS spectrum of GNC-1 and GNC-2. (b) N1s and (c) S2p XPS spectrum of GNC-1.

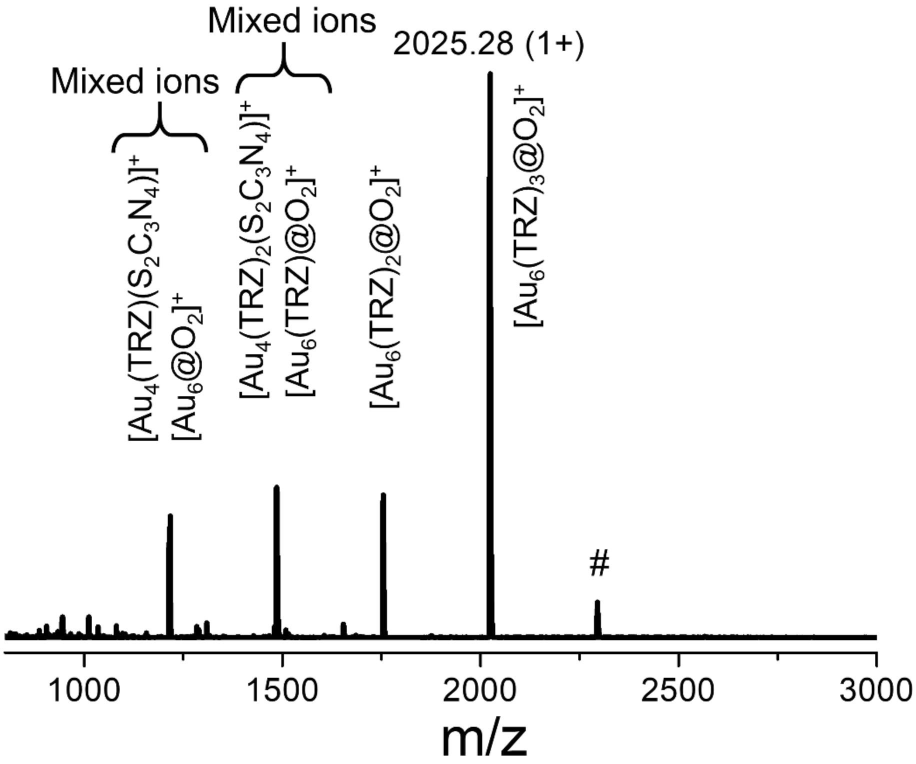

Figure S5. Full range ESI-MS spectrum of GNC-1 in positive ion mode. TRZ fragmentations were observed from the parent ion peak. The fragmentation of Au_6 core was also observed. The peak '#' indicates one TRZ attachment with the parent peak.

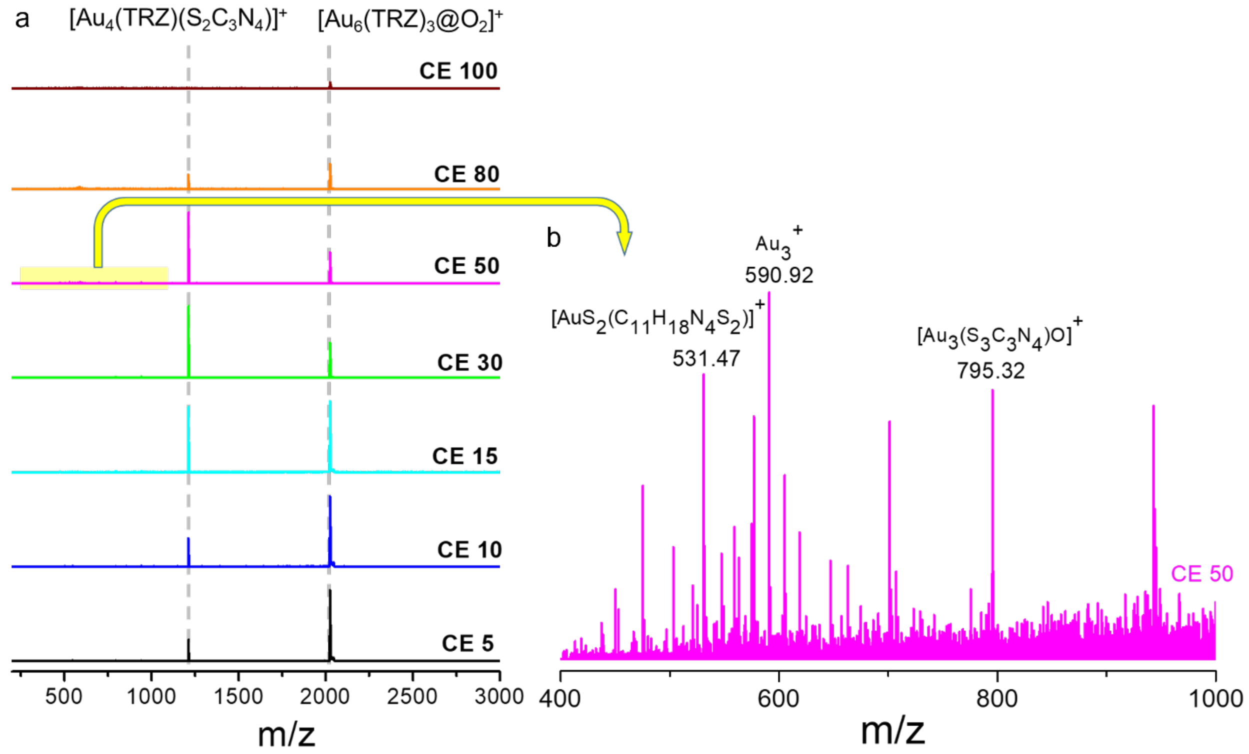

Figure S6. (a) The collision energy dependent fragmentation studies shows the formation of $[Au_4(TRZ)(S_2C_3N_4)]^+$ fragments from the parent cluster. (b) Expanded view of the lower spectral region shows other fragmented peaks.

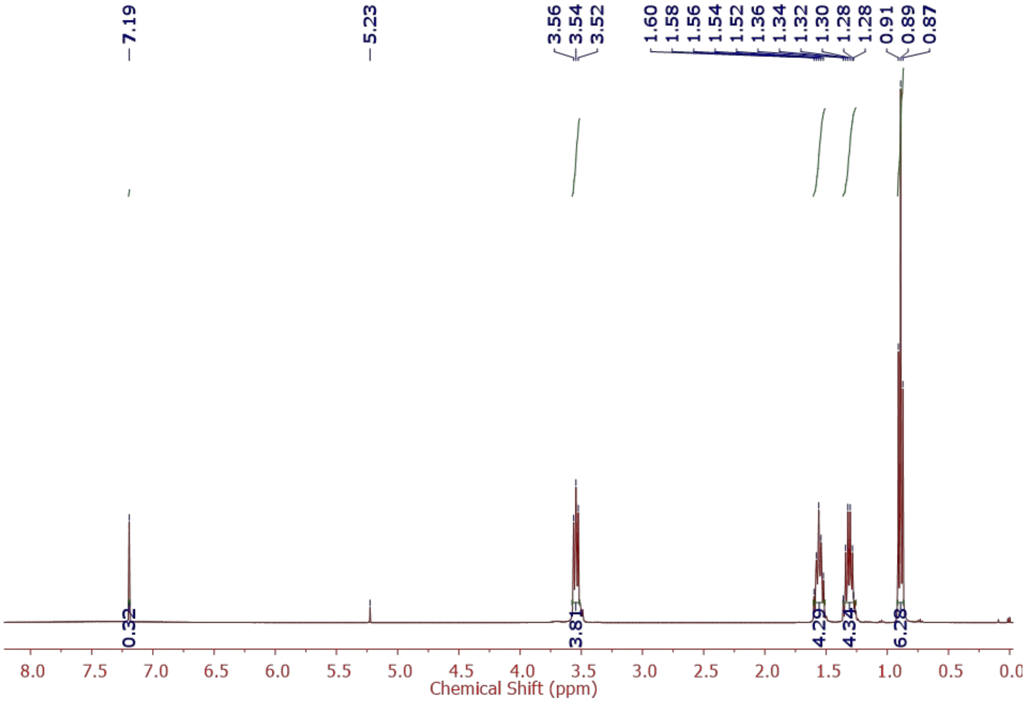

Figure S7. ^{1}H-NMR spectrum of the isolated TRZ ligand.

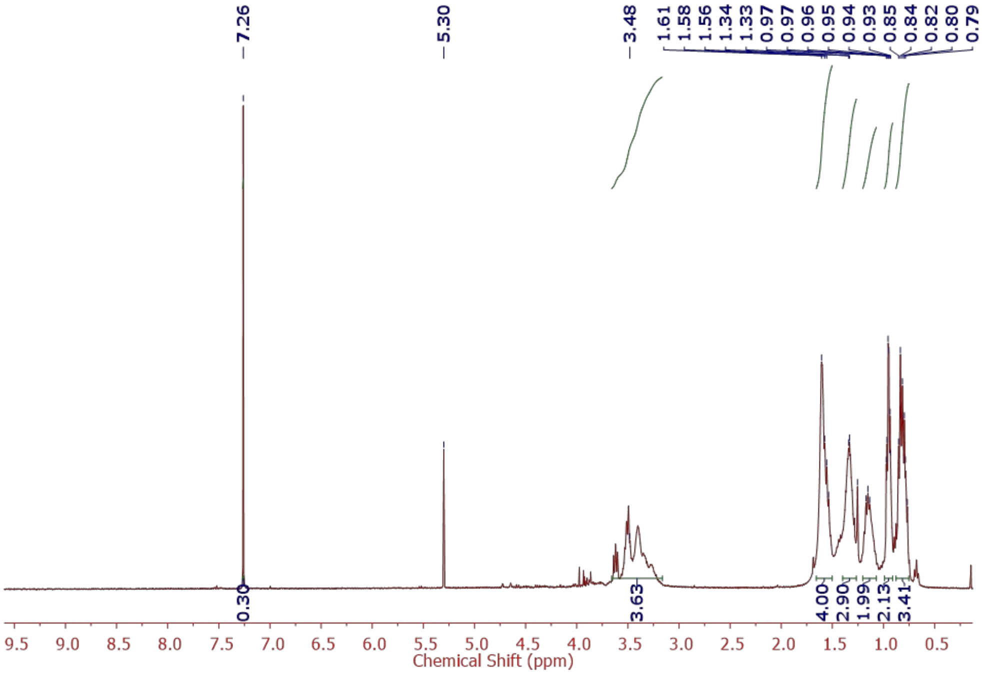

Figure S8. ^{1}H-NMR spectrum of the GNC-1.

The ^{1}H NMR spectrum of the ligand shows a peak at 7.19 ppm, probably due to the NH^+ proton. The absence of ^{1}H resonance signals between 2-3 ppm region, indicates deprotonation from the -SH group (i.e., the same proton is bound to nitrogen atoms). Upon binding the ligands with the Au_6 core, peak broadening was not observed for the NH^+ peak. However, broadening of the peaks corresponding to butyl protons was observed due to electron dense Au atoms. Direct covalent bonding of the butyl chains through the nitrogen center strongly influences the easy delocalization of electrons to these hydrogens.

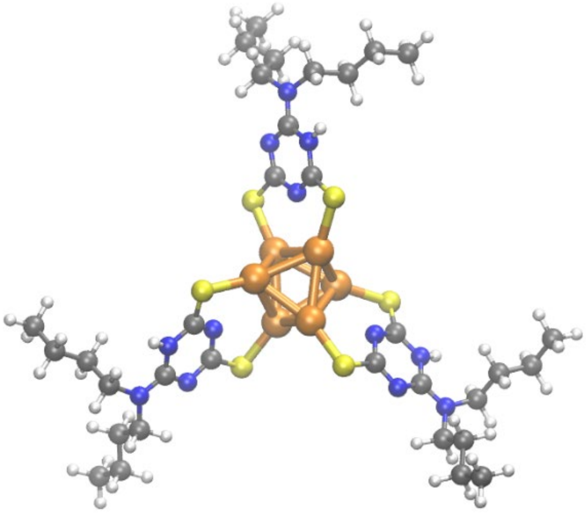

Figure S9. The atomic structure of $[Au_6(TRZ)_3]^+$ optimized by DFT.

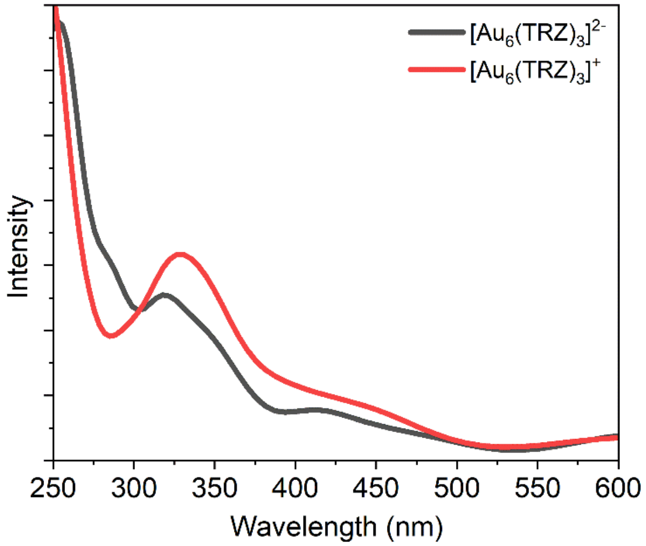

Figure S10. The TDDFT calculated optical absorption spectra of $[Au(I)_6(TRZ)_3]^{2-}$ and its protonated $[Au(I)_6(TRZ)_3]^+$ nanoclusters.

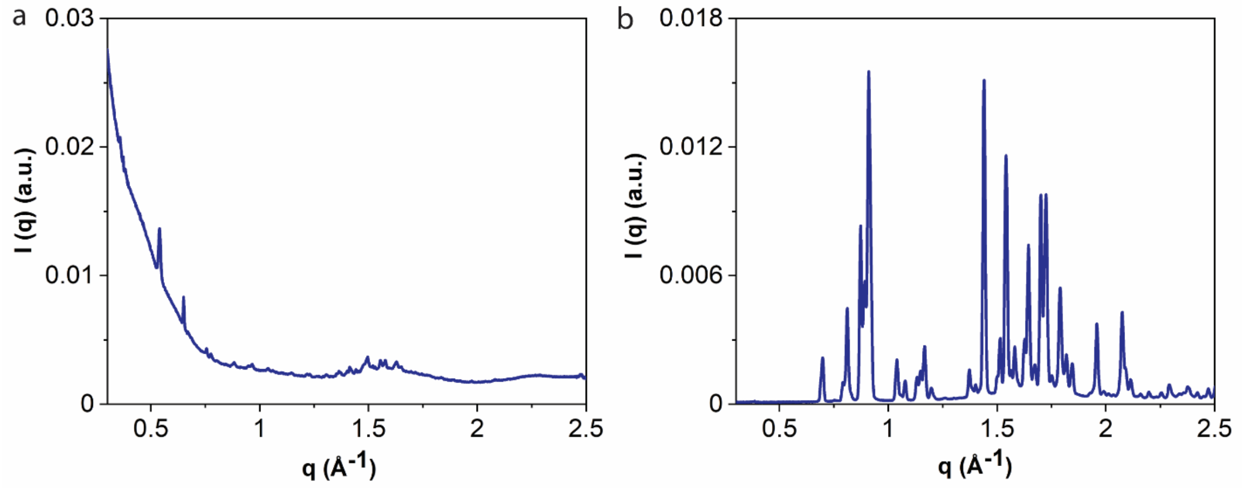

Figure S11. Small angle X-ray diffraction (SAXS) pattern of (a) GNC-1 and (b) isolated TRZ ligand.

The small angle X-ray diffraction (SAXS) of NCs produced distinct diffraction peaks in the range 0.5 to 2 Å^{-1} on a baseline with broad maxima and shoulders. The SAXS results support the octahedral structure of $Au(I)_6$ NCs (Figure S11a). The baseline shape cannot be unambiguously correlated with any specific structure, and it reflects the less ordered fraction that results from the rapid drying of DCM. The comparison of the SAXS pattern of pure ligand without gold (Figure

S11b) confirms that the diffraction peaks from the nanocluster sample are not arising from excess starting components.

The input parameters for diffraction pattern calculation:

Unit cell dimension: *a* = 11.85 Å, *b* = 9.81 Å, *c* = 8.37 Å

Unit cell angles: alpha = 85.700 deg., beta = 85.300 deg., gamma = 98.200 deg.

Atom	N	*a* coordinate	*b* coordinate	*c* coordinate
Au1	79	0.3305 0.0000	0.0000	
Au2	79	0.6695	0.0000	0.0000
Au3	79	0.5061	0.1287	0.1707
Au4	79	0.4715	0.8362	0.1707
Au5	79	0.5285	0.1638	0.8293
Au6	79	0.4939	0.8713	0.8293

RGNR 1

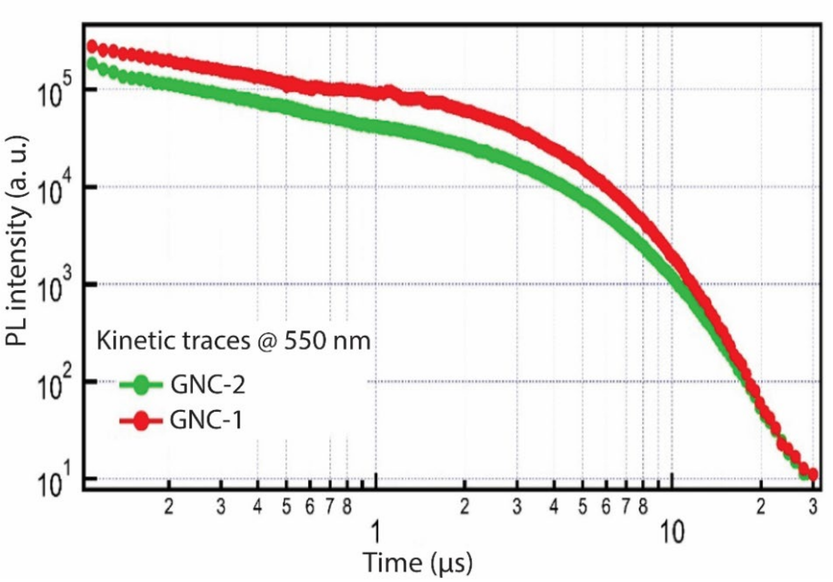

Figure S12. Decay kinetics of the spectrally integrated PL signal of GNC-1 (red line) and GNC-2 (green line).

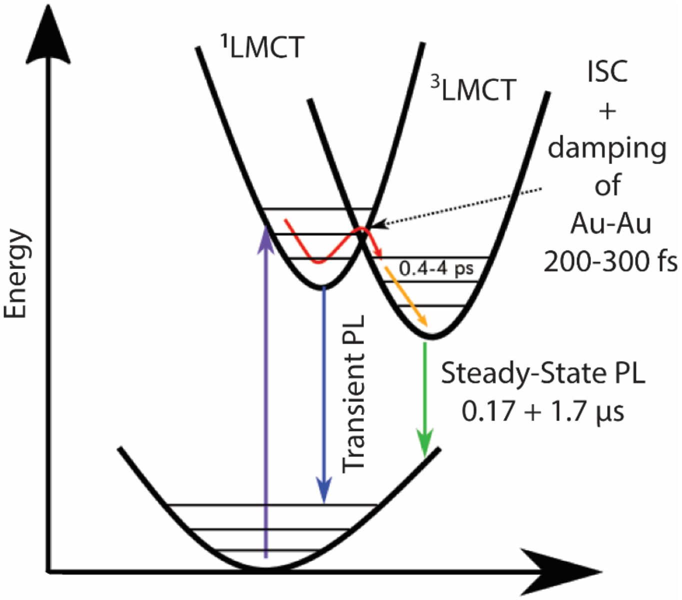

Figure S13. Photocycle of GNCs.

Calculation of third order nonlinear susceptibility:

The third order nonlinear susceptibility is calculated at 1300 nm wavelength with the formula given as:

$$\chi^{(3)} = \frac{4\varepsilon_0 c^2}{3\omega d}\sqrt{n_\omega^3 n_{3\omega}\frac{I_{3\omega}}{I_\omega^3}}$$

Where ε_0, c and d are the permittivity of vacuum, speed of light in vacuum, and sample thickness respectively. n_ω ($n_{3\omega}$) and I_ω ($I_{3\omega}$) are the refractive index at frequency ω (3ω) and pump (THG) intensity respectively. The values are as follows:

$\varepsilon_0 = 8.845 \times 10^{-12}$ F/m

$c = 3 \times 10^8$ m/s

$n_\omega = 1.908$

$n_{3\omega} = 2.1684$

$I_\omega = 28.84$ GW/cm^2

$I_{3\omega} = 7.02$ KW/cm^2

d = 5 nm

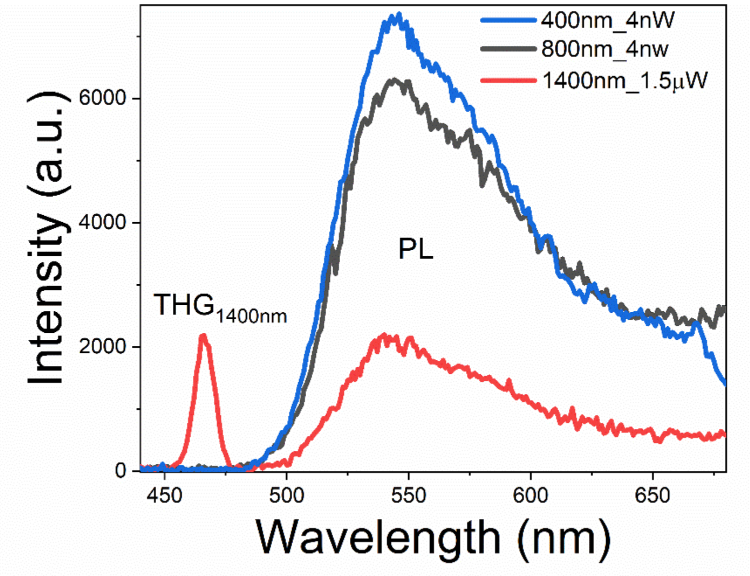

Figure S14. Multiphoton PL response of the thin film GNCs from pulsed laser of different wavelengths of excitation.

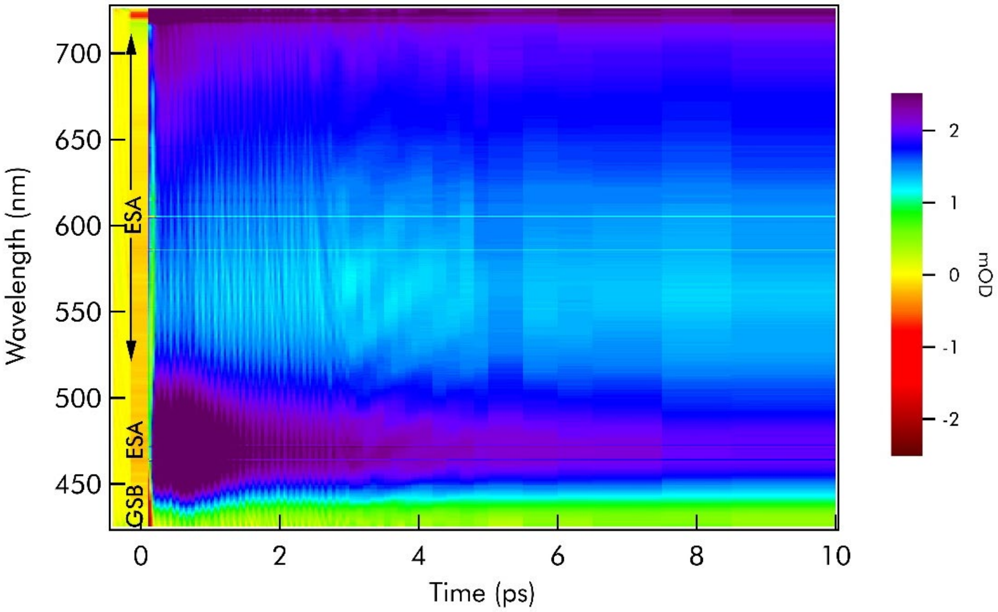

Figure S15. Time-wavelength contour plot of the TA signal of GNC-1 excited at 400 nm, shown in the first 5 ps.

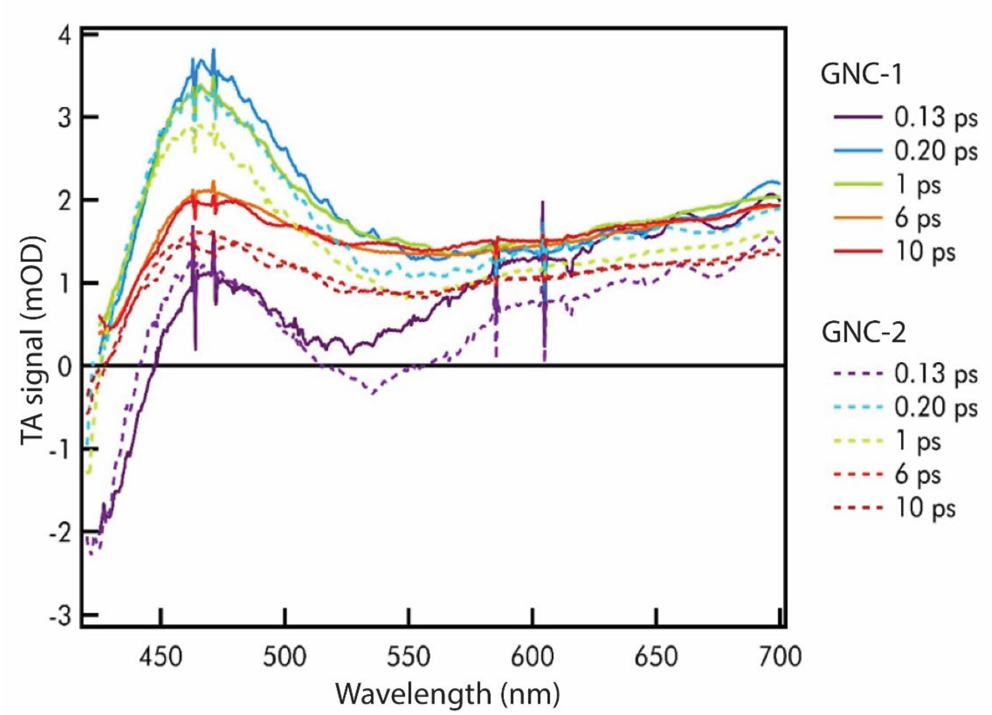

Figure S16. TA spectra at different pump-probe delays of GNC-1 (continuous lines) and GNC-2 (dashed lines).

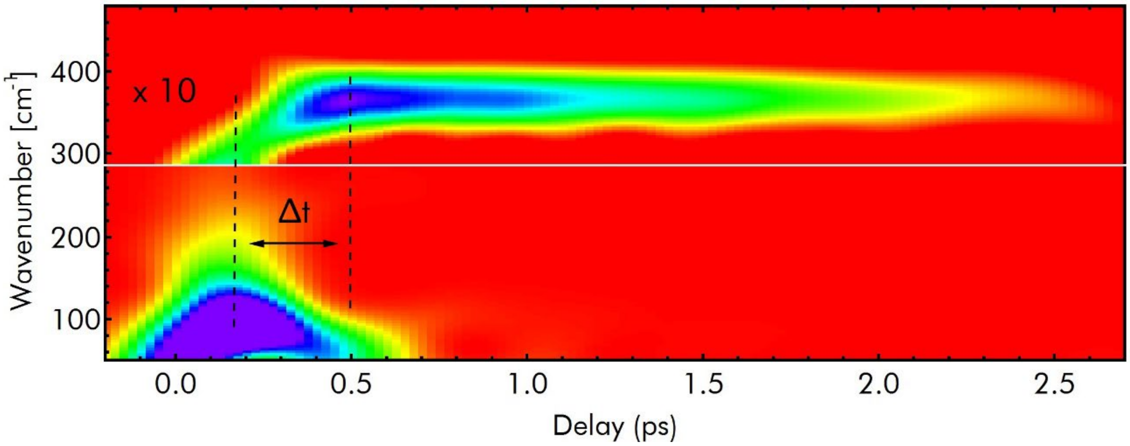

Figure S17. Time-frequency analysis of the fit residuals plotted in Figure 4d of the main paper, calculated as a short-time Fourier transform within a Hann moving window with 800 fs width (about twice the period of Au-Au oscillations).

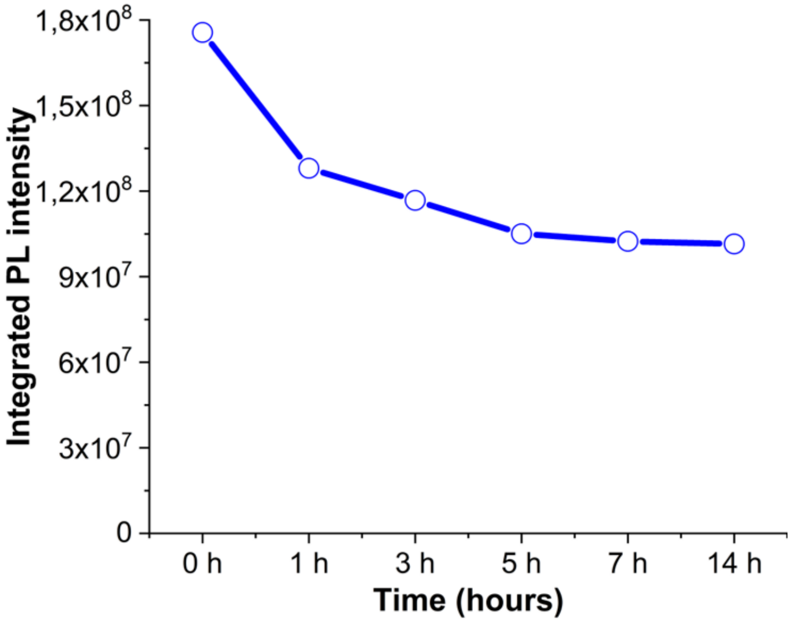

Figure S18. Photostability of GNC-1 under continuous exposure of UV light.

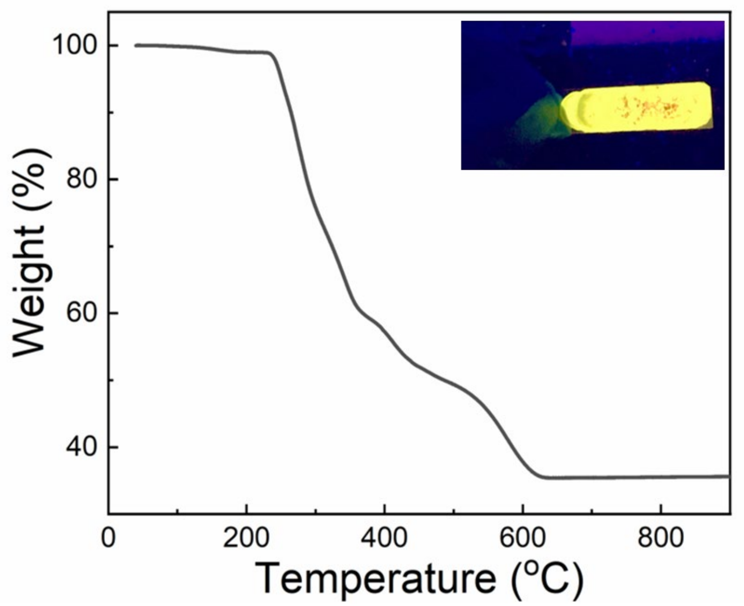

Figure S19. Thermogravimetric analysis (TGA) of GNC-1. Inset shows the GNC-1 film under UV exposure after treatment at 100 ºC for 1 hour.

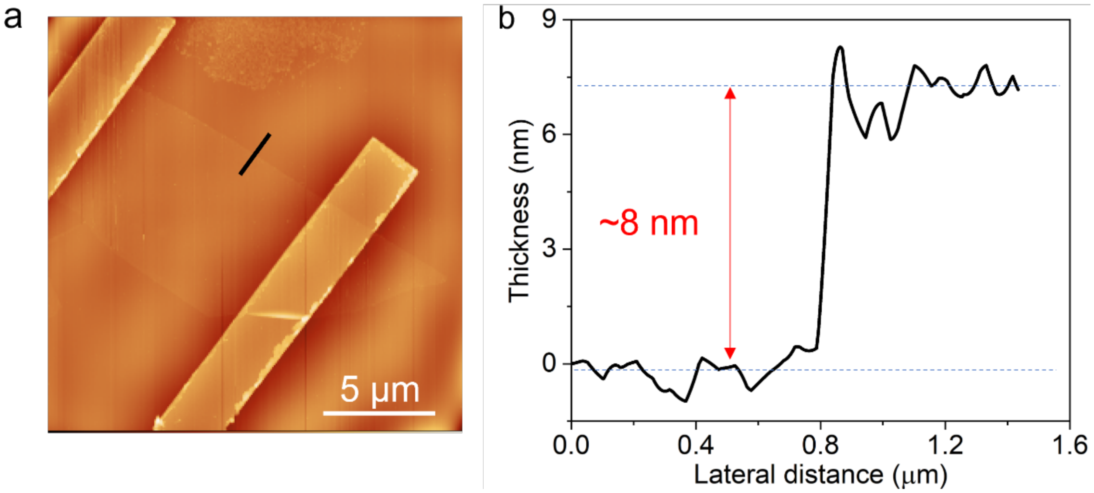

Figure S20. Thickness extraction of WSe_2 flakes. (a) Topographic image of pristine WSe_2 devices obtained by atomic force microscope. (b) Height profile of WSe_2 flake collected across black line indicated in (a).

References:

[1] W. Kraus, G. Nolze, *J. Appl. Crystallogr.* **1996**, *29*, 301–303.

[2] A. Sciortino, F. Ferrante, N. Mauro, G. Buscarino, L. Sciortino, G. Giammona, M. Cannas, D. Duca, F. Messina, *Carbon N. Y.* **2021**, *173*, 454–461.

[3] J. Enkovaara, C. Rostgaard, J. J. Mortensen, J. Chen, M. Dułak, L. Ferrighi, J. Gavnholt, C. Glinsvad, V. Haikola, H. A. Hansen, H. H. Kristoffersen, M. Kuisma, A. H. Larsen, L. Lehtovaara, M. Ljungberg, O. Lopez-Acevedo, P. G. Moses, J. Ojanen, T. Olsen, V. Petzold, N. A. Romero, J. Stausholm-Møller, M. Strange, G. A. Tritsaris, M. Vanin, M. Walter, B. Hammer, H. Häkkinen, G. K. H. Madsen, R. M. Nieminen, J. K. Nørskov, M. Puska, T. T. Rantala, J. Schiøtz, K. S. Thygesen, K. W. Jacobsen, *J. Phys. Condens. Matter* **2010**, *22*, 253202.

[4] J. P. Perdew, K. Burke, M. Ernzerhof, *Phys. Rev. Lett.* **1996**, *77*, 3865–3868.

[5] A. Tkatchenko, M. Scheffler, *Phys. Rev. Lett.* **2009**, *102*, 6–9.

[6] M. Kuisma, A. Sakko, T. P. Rossi, A. H. Larsen, J. Enkovaara, L. Lehtovaara, T. T. Rantala, *Phys. Rev. B - Condens. Matter Mater. Phys.* **2015**, *91*, 115431.

[7] E. Kalered, N. Brenning, I. Pilch, L. Caillault, T. Minéa, L. Ojamäe, *Phys. Plasmas* **2017**, *24*, 013702.